

BEAM DYNAMICS IN THE LOW ENERGY PART OF THE LOW EMITTANCE GUN (LEG)

M. Dehler, S. G. Wipf, Paul Scherrer Institut, Switzerland

Abstract

One option for the electron source of the SwissFEL is the Low Emittance Gun (LEG), which is currently under development at PSI. It consists of a pulsed DC gun operating at 500 keV and has the option of using either a photo cathode or a field emitter array. The gun is followed by a pulsed in-vacuum solenoid and a two-frequency cavity, not only used to accelerate the beam but also to create a highly linear energy correlation required for ballistic bunching. All components are rotationally symmetric, so a full particle-in-cell simulation of the setup using 2 1/2 D MAFIA, including space charge, wake fields and beam loading effects, shows the base line performance. Given the relatively low beam energy and high brightness of the beam, there were concerns with respect to the sensitivity to mechanical misalignments in the structure. So we investigated these using the 3D in-house code CAPONE and calculated tolerances, which are well within acceptable limits.

INTRODUCTION

To realize compact X-ray free electron lasers, electron sources with a high brilliance and ultra low emittance are required. The SwissFEL project at PSI is based on the development of such concepts, allowing a substantial reduction in size and cost of such a facility. In order to reach the Angstrom wavelength range, peak currents of 1.5 kA, a relative energy spread of 10^{-4} and normalized transverse slice emittances in the order of 300 nm rad are crucial in the standard operation mode.

Several options are under discussion for the electron source. One consists of an S-band RF gun with a photo cathode[1] running at gradients of 100 MV/m, which will be tested in the 250 MeV injector facility currently under construction. The other, examined here, employs a pulsed diode at an accelerating gradient of 125 MV/m gradient over a four millimeter gap[2], where a prototype is under commissioning at PSI. The baseline scenario assumes a photo-cathode, but cathodes using field emitter arrays may be promising candidates[4, 5].

Even after the high gradient acceleration in the diode, the electron beam is still fragile at energies of 500 keV. A low initial beam current of 5.5 A with an overall charge of 200 pC is beneficial in that respect, but requires a large bunch compression ratio of 270 to obtain a peak current sufficient for lasing. Therefore after the diode, the electron beam is accelerated off-crest in a two-frequency cavity. The fundamental mode at 1.5 GHz is combined with a higher har-

RF Guns and Linac Injectors

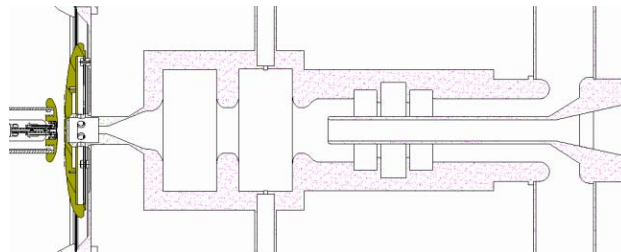


Figure 1: Pulsed DC gun with dual frequency cavity (solenoid not visible)

monic at 4.5 GHz to introduce a highly linear energy chirp to do ballistic bunching in the following drift delivering a peak current of 20 A to the linac. The beam current and phase space at the end of the drift are compatible with those expected from the S-band RF gun option, so that we can use the same linac design for both options. Fig. 1 shows the layout. A pulsed solenoid (not shown in the figure) between diode and two-frequency cavity corrects the residual divergence of the beam after the gun.

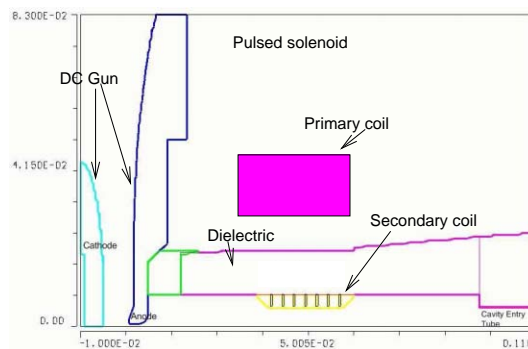


Figure 2: Diode and pulsed solenoid

The simulations have been performed in two steps. Since all elements are rotationally symmetric, the base line performance assuming perfect alignment and ideal beam properties is obtained from a 2½D particle in cell simulation using MAFIA TS2[6]. The influence of misalignment, beam offsets etc. was obtained with the in-house code CAPONE[7] and is described in a separate section.

BASE LINE PERFORMANCE

As was mentioned above, the assembly is rotational symmetric, so it was modeled in two dimensional cylindrical coordinates. The setup consists of the following, the cath-

ode and anode disks, followed by a pulsed solenoid and the dual-frequency cavity. To be able to resolve the space charge of the particles within the thin bunch, the mesh is very fine especially close to the z-axis with a minimum resolution of $33 \mu\text{m}$ and an overall grid size of 250,000 points, at which the full numerical convergence of the results was obtained. The nominal gap between anode and cathode is 4 millimeters. Both were modeled as precise as possible in order to obtain sufficient resolution for the fine detail of the surface shape. The diode voltage is 500 kV giving an average accelerating gradient of 125 MV/m.

The solenoid (Fig. 2) is a corrugated steel insert sitting inside the ceramic beam pipe. The azimuthal magnet current is excited in this insert by magnetic induction via a secondary coil indicated in the figure. While the beam is passing through the magnet, the resulting field can be assumed as constant, though with important differences to the field distribution of a truly static magnet. Where the magnetostatic field is determined by the distribution of the driving currents and the permeability, we have the additional influence of induced mirror current on the various conducting parts as e.g. the anode plate or the RF cavity resulting in a shielding effect.

The PIC module in MAFIA can use only static focusing fields, so we employed the following strategy to arrive at a realistic field distribution. The metallic insert corresponding to the winding of the solenoid carries a homogeneous current distribution, something which we can safely assume from the material properties and the time domain behavior of the driving pulse. All metallic parts were specified with a very low permeability of 0.01 to push out the magnetic fields. Furthermore, a tiny shielding current (also homogeneously distributed) was assumed in the anode plate and set to a value minimizing the magnetic field between anode and cathode¹. Figure 3 shows the on-axis distribution of the longitudinal field.

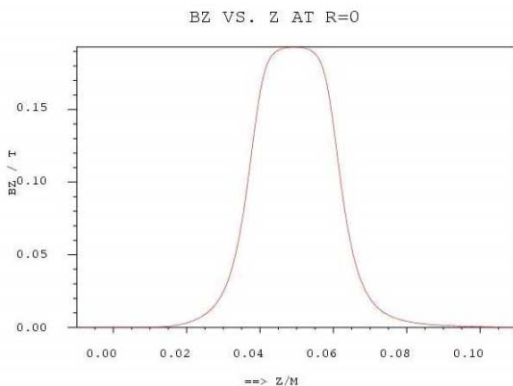


Figure 3: On axis field of pulsed solenoid

With the given parameters (0.5 kV and a 4 mm gap at the pulser), the solenoid needs a focusing field strength of

¹A fully realistic computation could only be done in 3D with the help of a time domain computation, but we still would need special tricks to load the field into the PIC simulation.

$\int B_z^2 dz = 0.92 \cdot 10^{-3} T^2 m$ to correct for the residual divergence of the beam after the DC gun.

The cavity was modeled including the subsequent filter section. The entry of the RF-Cavity fits into the end of the solenoid. The cavity is designed so that the third harmonic RF mode, TM_{012} can be superimposed on the fundamental one, the TM_{010} . Apart from acceleration, the fundamental frequency provides the energy chirp for compression. The higher harmonic serves to linearize the longitudinal phase space. Initial beam and field parameters used in the simulation are listed in table 1.

Table 1: Initial parameters used in simulation

Emittance	70 nm rad
Beam diameter (homogeneous)	600 μm
Energy	$\gamma=1.0003$
Pulse length (flat top)	40 ps
Beam current	5.5 A
Gun voltage	500 kV
Slice length for sliced emittance	1 ps
Solenoid strength	$0.92 \cdot 10^{-3} T^2 m$
Fundamental mode	
Amplitude	35.5 MV/m
Phase/deg.	-15
Harmonic mode	
Amplitude	17 MV/m
Phase/deg.	10

The field values for the solenoid and the RF cavity differ from the official parameter set in the CDR[2] for the following reasons. First, we used the latest structure geometries, which differ from those used in generating the reference case. When trying to find a good beam behavior in the vicinity of the reference value, we saw that the beam behavior is very sensitive to small variations in the input parameters. This is due to the fact that the beam at the entry of the RF structure is simultaneously focused in the transverse plane and sees a deceleration in the order of 30%, so that space charge effects become quite pronounced. We went to a new working point and reduced the phase of the fundamental mode by roughly 20 degrees to $\phi = -15$ degrees and increased the amplitude of the harmonic mode from 11 to 17 MV/m. The pronounced drop in beam energy at the entrance of the cavity is strongly reduced leading to a more stable behavior. The resulting longitudinal phase space obtained by either accelerating only with the fundamental mode or with both is shown in Fig. 4. The combination of both modes results in a nicely correlated energy spread suitable for ballistic compression in the following drift.

The big bump in emittance, as the bunch is traversing the solenoid (Fig. 5), may be irritating, but it is due to the fact that the code (as well as all other known codes) only uses the kinetic transverse momenta to compute emittances. A computation using the generalized momentum $p = mv + qA$ would not show this behavior. Only the

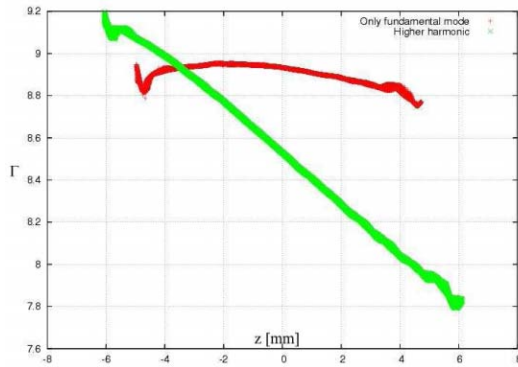


Figure 4: Longitudinal phase space at exit of the dual-frequency cavity ($z = 370\text{mm}$) with/without harmonic mode

emittance values outside the solenoid region are relevant.

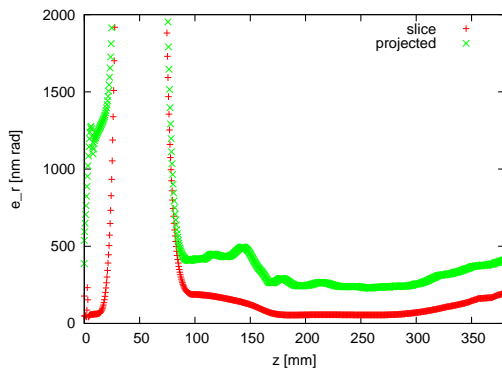


Figure 5: Evolution of slice and projected transverse emittance during flight.

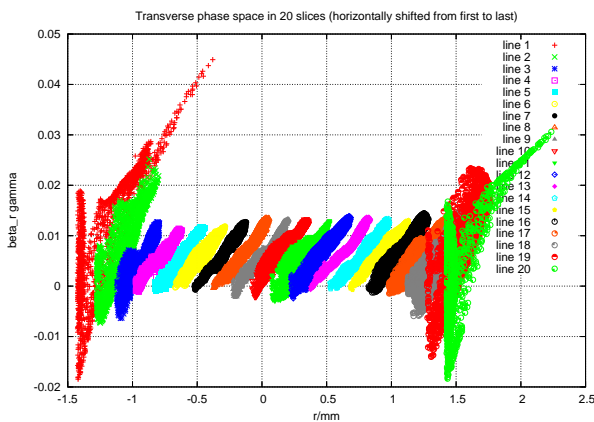


Figure 6: Phase space distribution of individual bunch slices at the exit of the dual-frequency cavity ($z = 370\text{mm}$)

The best view of the transverse phase space distribution is obtained by looking at individual slices in the bunch. In Fig. 6, the distribution of several slices is shown with the leftmost corresponding to the tail slice and the rightmost to

RF Guns and Linac Injectors

that of the head of the bunch. We have a very good emittance of the center slices corresponding to values slightly above 180 nm rad. Only the outermost slices see a deterioration due to nonlinear space charge, RF forces as well as wake fields. The angle of the phase space ellipses of the center slices are very well aligned with respect to each other, so that there is no intrinsic emittance increase by subsequent bunch compression stages merging adjacent slices. Table 2 lists the beam parameters seen after the RF structure.

Table 2: Beam parameters at the exit of the RF structure ($z = 370\text{mm}$)

Parameter	Center slice	Projected
$\epsilon_t/\text{nm rad}$	176	378
$\epsilon_z/\text{eV s}$	$1.2 \cdot 10^{-9}$	$3.9 \cdot 10^{-1}$
$\sigma_r/\mu\text{m}$	297	272
$\sigma_{r'}/\text{mrad}$	1.0	1.0
γ/MeV	3.9	3.9
σ_t/ps	0.25	10.8
$\sigma_\gamma/\%$	0.12	4.7

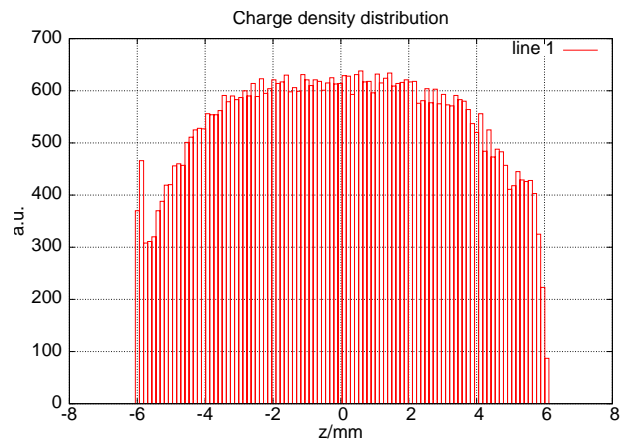


Figure 7: Intra bunch charge density at exit of the dual-frequency cavity ($z = 370\text{mm}$)

Fig. 7 shows the relatively flat charge distribution inside the bunch. The small scale fluctuations seen are due to numerical noise. The peak at the bunch tail ($z = -6\text{mm}$) is a numerical artifact due to the code.

MISALIGNMENTS

Including misalignments as structure offsets or tilts into the simulations destroys the symmetry of the problem, so a full three dimensional simulation has to be performed. To do that, we used the in-house particle-in-cell code CAPONE, which was originally developed to do ultra high resolution of electron sources based on field emission arrays[7]. The original version was restricted to have only static accelerating fields, whereas here we also need to take into account time harmonic fields.

Running an eigenvalue solver on the large grid sizes of an order of a billion mesh cells required to have a consistent field solution for the particle-in-cell algorithm is a rather tedious task – the more, since we need not only the fundamental mode in the RF structure but also the third harmonic. With the typical three dimensional solver, this means computing all modes of all azimuthal orders up to that frequency, so that approximately 100 modes need to be determined.

A rather elegant alternative was to introduce 2D field maps into CAPONE allowing the use of high resolution two dimensional solution. These are not distributed into the three dimensional calculation grid but kept in 2D format and read out there by the force calculation routine. Apart from the easier generation of these fields, this has other significant advantages. For one, the domain spanned by the grid for the particle-in-cell solver does not have to extend over the full volume of e.g. the RF cavities, but can be truncated to the size relevant for a correct representation of space charge fields and wakes. This feature can reduce the size of the particle-in-cell grid already considerably. As a second feature, we can easily introduce misalignments as offsets or tilts by simply moving the 2D field map with respect to the PIC grid.

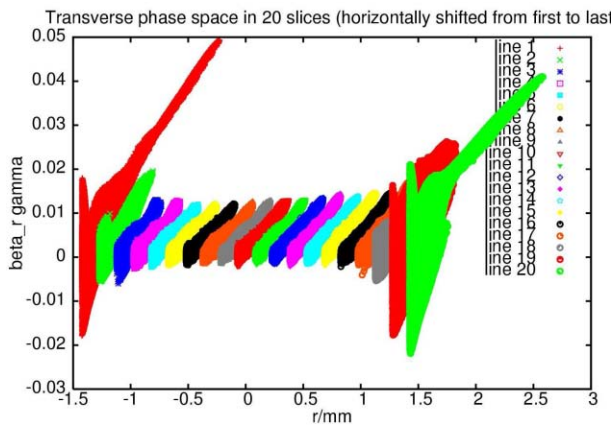


Figure 8: Phase space distribution of bunch slices as calculated with CAPONE ($z = 370\text{mm}$)

The initial conditions for the beam correspond to that of the two dimensional case (Tab. 1) with the exception of the longitudinal profile. In the three dimensional calculation, the flat top profile had a non zero rise and fall time of 0.5 picoseconds. 2D and 3D results agree well, we have normalized emittance values of 388 nm-rad in 2D versus 383 nm-rad in 3D. The one significant difference is seen in the center slice emittance, where we obtain 170 nm-rad in 2D compared to 120 nm-rad in 3D, which is probably due to artifacts in the stochastic distributions used in MAFIA as shown in Fig. 7. Fig. 8 shows the 3D slice emittances at the exit of the cavity.

For the various misalignments, the following cases were computed: The laser spot on the cathode was assumed to be misaligned by $300\ \mu\text{m}$, the solenoid was calculated with

RF Guns and Linac Injectors

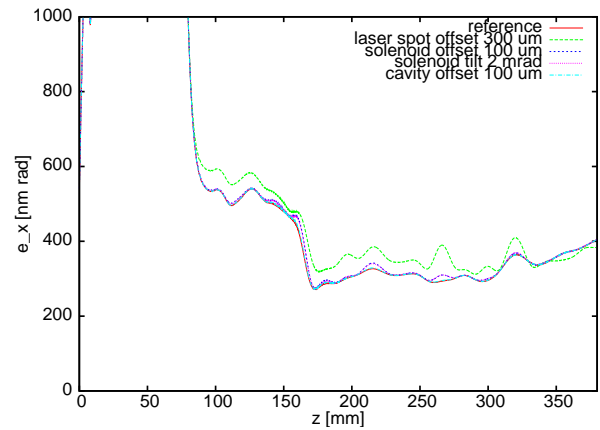


Figure 9: Envelope of the projected transverse emittance for various misalignments.

offset ($100\ \mu\text{m}$) and tilted ($2\ \text{mrad}$) and the effect of an offset of the cavity of $100\ \mu\text{m}$ was simulated.

The variation of the projected emittance is relatively minor as can be seen in figure 9. Only the rather extreme offset of the laser spot leads to a visible difference. Similar is the influence on the center slice emittance. The only significant deterioration is visible, if we start with an offset beam. Fig. 11 shows the phase space distribution for the case of a shifted laser spot.

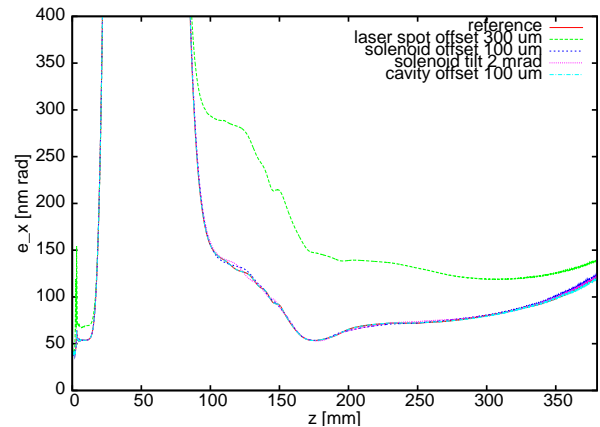


Figure 10: Envelope of the slice emittance in the bunch center for various misalignments.

Does this mean, that misalignment is a non-issue for the setup? In addition to any widening of the phase space volume occupied by the bunch, the kicks introduced by the finite tolerance lead to a displaced of the bunch centroid in the transverse phase space as can be seen in Fig. 12 and Fig. 13 for the mean position and flight angle respectively, which lead to mismatching in the following beam optics.

In principle, one can correct this effect by additional corrector magnets, but one could also try to find tolerances rendering these correctors unnecessary. The required criterion is, that the displacement of the bunch centroid still fits into the maximum allowable phase space volume (aka

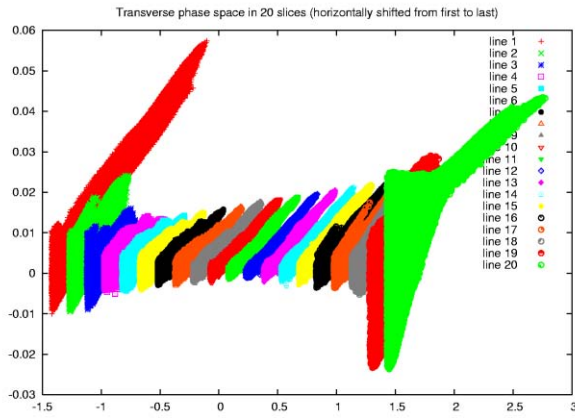


Figure 11: Phase space of bunch slices assuming a shifted laser spot.

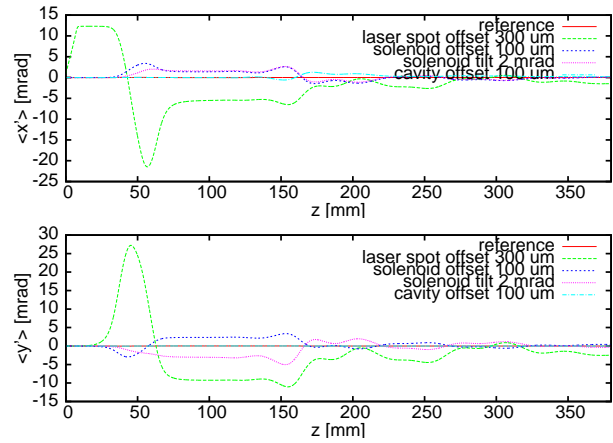


Figure 13: Variation of beam angle along beam axis

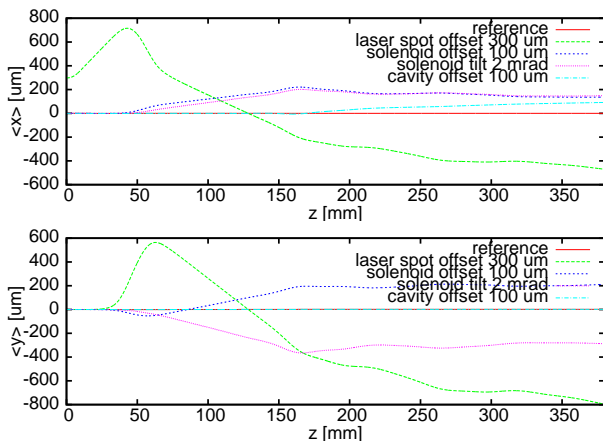


Figure 12: Variation of beam offset along beam axis

projected emittance) of the bunch of roughly 400 nm-rad. Given the geometrical offsets $\langle x \rangle$, $\langle y \rangle$ and momentum offsets $\langle u_x \rangle$ and $\langle u_y \rangle$, we can define a kind of a pseudo emittance

$$\epsilon_p = \sqrt{(\langle x \rangle \langle u_x \rangle)^2 + (\langle y \rangle \langle u_y \rangle)^2},$$

which by definition should be lower than the limit of the projected emittance. Fig. 14 shows envelopes of this pseudo emittance for the different cases of misalignment. ϵ_p scales roughly quadratically with offset or tilt, table 3 uses this relationship to derive alignment tolerances.

Table 3: Alignment tolerances to keep pseudo emittance below 400 nm

Parameter	Tolerance
laser spot offset	45 μm
solenoid offset	70 μm
solenoid tilt	1.3 mrad
cavity offset	140 μm

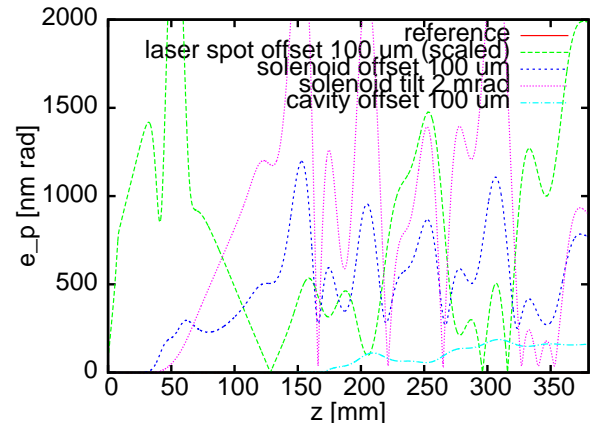


Figure 14: Envelope of the pseudo emittance ϵ_p (definition see main text) for various misalignments.

CONCLUSIONS

A simulation of the Low Emittance Gun (LEG), comprising the pulsed DC source at 500 kV, the pulsed solenoid and the two frequency cavity, has been completed. If one compares the settings and results with those in the official specification[2], the following remarks have to be made. Using the official parameter set, we see (as in up-to-date simulations by Anne Oppelt with tracking codes[8]), that the setup is extremely sensitive to minor variations in phase and amplitude of the cavity modes. At the entrance of the cavity the beam energy drops considerably, this is due to the fact that it is strongly focused, so that space charge forces are quite dominant. Given a run time of the simulation of 6-8 CPU hours and a corresponding limited number of possible iterations, it was not possible to find a satisfactory solution in the vicinity of the official parameters. In the end, a different working point was found, where the beam is more on the crest of the fundamental mode and which has the following advantages: The drop in beam energy at the entrance of the cavity is visibly reduced and the radius and projected emittance at the exit are lowered. If one compares emittance values computed by tracking codes such as

BET (beam envelope tracker)[9] with those of a particle in cell simulation, one sees the following: Slice parameters in the bunch center agree relatively well, but the tracking codes do underestimate the deterioration seen by the head and tail of the bunch, so that the PIC code computes a larger value for the projected emittance.

Using the in-house code CAPONE, the influence of mis-alignments on the performance has been calculated. Other than the setting of amplitudes and phases for the RF cavity mentioned above, tolerances for the geometrical alignment of the setup are relatively relaxed for the operation.

REFERENCES

- [1] Y. Kim et al., “Linear Accelerator for the PSI-XFEL FEL3 Beamline”, Proc. of the LINAC 2008, Vancouver, Canada (2008)
- [2] A. Oppelt et al., “Towards a low emittance X-ray FEL at PSI”, Proc. of the 2007 Free-Electron Laser Conference (FEL2007), Novosibirsk (Russia)
- [3] J.-Y. Raguin et al., “A two-frequency RF cavity for the PSI-XFEL: Design and beam dynamics simulations”, Nuclear Instruments and Methods in Physics Research A 593 (2008) 125 128
- [4] E. Kirk et al., “Development of All-metal Field Emitter Arrays for high Current Applications”, proc. International Vacuum Electronics Conference, May 15-17, Kitakyushu, Japan (2007)
- [5] M. Dehler et al., “Full scale simulation of a field-emitter arrays based electron source for free electron lasers”, J. Vac. Sci. Technol. B 24 (2), pp. 892-897 (2006)
- [6] <http://www.cst.de>
- [7] A. Candel, M. Dehler, “Massive parallel particle in cell code for the simulation of field emitter based electron sources”, proc. 8th International Computational Accelerator Physics Conference, Jun. 29- Jul. 02, St. Petersburg, Russia (2004), Nucl.Instrum.Meth.A558:154,2006
- [8] A. Oppelt, personal communication
- [9] R. Bakker, PSI in-house development.